Hindawi
Structural Control and Health Monitoring
Volume 2024, Article ID 6631877, 18 pages
https://doi.org/10.1155/2024/6631877

Research Article

Transformer-Enhanced Traffic Load Simulation for Wear Evaluation of Bridge Expansion Joint

Yiqing Dong,[1,2] **Yue Pan**,[1] **Dalei Wang**,[1,3] **and Airong Chen**[1]

[1]*College of Civil Engineering, Tongji University, Shanghai 200092, China*
[2]*School of Civil and Environmental Engineering, Nanyang Technological University, Singapore 639815*
[3]*Key Laboratory of Performance Evolution and Control for Engineering Structures (Ministry of Education), Tongji University, Shanghai 200092, China*

Correspondence should be addressed to Yue Pan; pan_yue@tongji.edu.cn

Received 15 November 2023; Revised 13 February 2024; Accepted 4 March 2024; Published 12 March 2024

Academic Editor: Andrea Del Grosso

Timely wear evaluation is crucial in maintaining the functionality of bridge expansion joints (BEJs), ultimately ensuring the safety of bridges. Despite the significance of traffic load simulation (TLS) in simulation-based evaluation methods, existing TLS approaches face challenges in accurately modeling in situ traffic flow at a high fidelity. This paper presents a novel methodology and its application for evaluating the wear performance of BEJs, employing a Transformer-enhanced TLS approach. Initially, a tailored dataset is crafted for data-driven car-following modeling, leveraging an established spatial-temporal traffic load monitoring system. High-fidelity TLS with a mean absolute error (MAE) of 0.1738 m/s is then achieved using Transformer modules equipped with an attention mechanism. To evaluate the final wear life of BEJs, transient dynamic analysis and a calibrated finite element model of the bridge are employed to extract cumulative displacement. Additionally, a surrogate model is developed to depict the relationship between the hourly traffic weight on the entire bridge deck and the cumulative displacement of BEJs, yielding an impressive R-squared value of 0.96619. Comparative results demonstrate the superior performance of our proposed TLS approach over other data-driven approaches, with the linear model derived from our TLS approach outperforming the model generated by the conventional Monte Carlo-based TLS approach. To conclude, our proposed TLS emerges as a comprehensive and precise methodology for the wear evaluation of BEJs.

1. Introduction

Bridge expansion joints (BEJs) constitute integral structural components designed to enable bridges to accommodate thermal movements and vibrations induced by traffic loads, wind forces, and seismic activities. However, the wear of slide bearings has emerged as one of the most frequent failure incidents for BEJs in long-span bridges, resulting in a service lifespan for BEJs that is considerably shorter than that of the bridge itself. Therefore, it is imperative to employ effective and predictive wear evaluation methodologies for BEJs to prevent structural damage and minimize additional maintenance costs [1, 2].

Although factors such as severe climatic conditions and unsuitable material components can influence the wear state, it has been confirmed that the primary cause of wear damage in BEJs is the cumulative displacement at the end of the girder [3–6]. Data analysis research, based on displacement gauges from structural health monitoring (SHM) systems, has been conducted. A variety of methods, including correlation fitting [3, 7–11], mechanical performance analysis of bridge structures [12–15], Bayesian approaches [16, 17], statistical machine learning [18], and data reconstruction [19, 20], have been utilized to examine the displacement patterns of BEJs for damage evaluation. The findings indicate that the wear damage of BEJs is primarily due to large cumulative displacements, which are significantly influenced by temperature and traffic loading. The temperature factor imparts a consistent trend to cumulative displacements and exhibits a linear relationship [9].

Conversely, traffic loading contributes significantly to the cumulative displacements of BEJs [3, 21]. However, traffic patterns are more spatially and temporally random, complicating the establishment of a relationship between traffic loads and cumulative displacements.

Despite the importance of SHM systems, the costs associated with their real-time installation and maintenance can be substantial. Moreover, wide-range gauges situated at the girder's end may operate at a low frequency (i.e., 2 Hz [7]), which presents difficulties in detecting displacement peaks and valleys, particularly when vehicles are entering or exiting the bridge. To address this issue, numerical simulation techniques have been introduced and applied for the wear evaluation of BEJs. These techniques integrate traffic loads with mechanical analysis. Considering the significance of traffic loads in the evaluation of BEJs, traffic load simulation (TLS) methods are vital as they offer substantial inputs for the analysis procedure. A commonly used TLS method is the Monte Carlo sampling of vehicle loads, which leverages data from the practical weigh-in-motion (WIM) system [22–24]. The recorded traffic load data undergo statistical analysis, and distribution equations of vehicle parameters are derived for subsequent TLS [25, 26]. Consequently, vehicles are generated based on statistical arrival times and traverse the lanes at constant speeds. Utilizing a finite element model (FEM) of the bridge structure, displacement histories and corresponding cumulative displacements are calculated to assess the wear performance of BEJs [3, 27]. To enhance the accuracy of displacement calculations, vehicle-bridge dynamic analysis has been incorporated into TLS [21].

However, the precision of TLS in these studies is somewhat compromised. This is primarily due to the inability of the Monte Carlo sampling-based method to consider vehicle interactions [28, 29]. Such interactions can induce speed fluctuations among vehicles, which in turn influence the distribution of traffic loads. Therefore, while these methods are widely accepted and utilized, they may not provide the high precision required for certain comprehensive bridge evaluations.

In recent years, microscopic traffic simulation approaches have been proposed, with a focus on the detailed description of each vehicle's movement on the road [30, 31]. These approaches aim to enhance the fidelity of traffic simulations, thereby improving the accuracy of structural evaluation procedures [32]. A key concept in microscopic traffic simulation is the car-following model, which takes into account the interactions between each pair of leading and following vehicles, thereby facilitating the simulation of comprehensive traffic flows on the road. Data-driven car-following models have gained increasing popularity in recent decades [33]. These models leverage traffic surveillance data to establish traffic flow characteristics. A multitude of studies have been conducted using a specific dataset known as the Next Generation SIMulation (NGSIM), provided by the Federal Highway Administration [34].

In terms of algorithms, to enhance the feature extraction capability of traditional models such as K-neighbouring [35], support vector machine (SVM) [36], and artificial neural networks (ANNs) [37], deep learning-based methods have been introduced and employed for the car-following prediction problem. The recurrent neural network (RNN) model, which takes into account the historical status of leading and subject vehicles, has been validated to simulate typical traffic phenomena [38]. Following this, models based on long short-term memory (LSTM) and gated recurrent unit (GRU) have been applied to the car-following prediction problem [39, 40] and have shown superior performance compared to the basic RNN model due to their more efficient memory cells [41]. Additionally, the Sequence-to-Sequence (Seq2Seq) and Encoder-Decoder architecture have demonstrated their advantages in multistep input and output performance [42, 43].

However, several challenges remain in the current TLS-based wear evaluation of BEJs, as detailed below. (1) Gaps exist between the microscopic TLS method and its practical application in the wear evaluation of BEJs and other bridge components. (2) There is an absence of a specific benchmarking dataset for data-driven TLS research related to long-span bridges. (3) Present data-driven vehicle trajectory prediction models encounter challenges in modeling long-term dependencies.

To address the challenges identified, this study presents a comprehensive methodology for evaluating the wear performance of BEJs using a Transformer-enhanced deep learning TLS approach. Specifically, a unique benchmarking dataset for data-driven TLS research is established, derived from a large-field traffic load monitoring system that employs machine vision and WIM data fusion. Furthermore, we propose a time-sequence model for predicting vehicle speed histories, which leverages Transformer modules to incorporate the attention mechanism, thereby recognizing long-term serial signal dependencies. Ultimately, precise wear evaluation of BEJs is achieved through transient dynamic analysis of the FEM of the long-span bridge. The primary contributions of this paper are four-fold. (1) We propose a data-driven methodology that facilitates a more precise wear evaluation of BEJs. (2) We provide a unique, first-of-its-kind dataset for benchmarking full-bridge TLS. (3) We develop a vehicle speed prediction car-following model for TLS, enhanced with Transformer modules within a deep learning framework, which achieves a low MAE. (4) We demonstrate that the linear surrogate model for BEJ wear evaluation, calibrated from the proposed TLS loading, outperforms conventional methods.

This paper is organized as follows. Section 2 introduces our proposed framework for the wear evaluation of BEJs, detailing the methods employed within the framework. In Section 3, we provide comprehensive information on benchmarking data collection and FEM verification for the bridge under study. The performance and feasibility of our model for high-fidelity wear evaluation of BEJs are presented in Section 4, along with discussions on comparative studies with existing models. Finally, Section 5 provides a conclusion, summarizing the key findings and implications of our research.

2. Methodology

2.1. Overview. This paper presents a methodology for evaluating the wear performance of BEJs using a Transformer-enhanced deep learning TLS approach. The methodology consists of three primary components, as depicted in Figure 1.

Initially, a spatial-temporal traffic load monitoring process is implemented using both visual and weighing sensors. A computer vision system, comprising multiple visual sensors, ensures complete coverage of the entire bridge deck. Identification algorithms are utilized to collect vehicle trajectory data. The WIM system, incorporating weighing sensors and induction coil sensors embedded within the pavement, is used to capture specific parameters of each passing vehicle, including its length, axle weight, and axle spacing.

Subsequently, a TLS approach, enhanced with deep learning and incorporating Transformer modules, is implemented. Following the initial phase, the vehicle trajectory data undergo a smoothing process and are segmented into car-following pairs. These pairs serve as the training data for the deep learning model for the prediction of the subject vehicle's speed. Concurrently, the vehicle weighing data are processed to determine the distribution of key parameters, such as vehicle arrival frequencies and axle weights. These distributions are then utilized to calibrate the Monte Carlo simulators for random sampling. The Monte Carlo simulators, in conjunction with the deep learning model, are then deployed for the generation of vehicles and the evolution of traffic on the bridge deck, respectively. This process results in the production of microscopic TLS data over a designated time.

Finally, the TLS data are sequentially incorporated into the FEM. Through the execution of a transient dynamic analysis, the displacement time histories of the girder's end are extracted. Ultimately, the cumulative displacements are computed to estimate the wear life of the BEJs.

2.2. Full-Span Traffic Load Acquisition. To complete the Transformer-enhanced data-driven TLS, the first requirement is the precise acquisition of on-deck traffic load, both spatially and temporally. Our previous studies [44, 45], which focused on a large-field traffic load monitoring system that utilizes the fusion of multivision and WIM sensing, have enabled us to acquire full-span traffic load flow. Briefly, as shown in Figure 2, our approach to traffic load acquisition incorporates both the WIM system and the computer vision system.

Within the WIM system, signals from both the induction coils and weighing sensors are processed. This involves the identification of impulse signals and the integration of time-sequence signals, respectively. As a result, we can determine the dimensions and axle weights of each vehicle. The WIM system, which is commercially available, has been actively collecting vehicle weight data since its installation.

In the case of the computer vision system, multiple high-definition cameras are mounted on the pylons to ensure complete coverage of the entire bridge deck. The video streams captured by these cameras are fetched, rectified, and stitched to generate a panoramic image flow of the bridge deck. These images are then processed using a trained YOLO-v4 object detector and a Kalman filter. The former is utilized to detect vehicles within the image flow and to obtain their respective coordinates and types. The latter is applied to track these vehicles based on the detections, thereby enabling the acquisition of their trajectories. For a more comprehensive understanding of the algorithms employed, readers are encouraged to refer to our previous studies [44, 45].

2.3. Microscopic TLS Scenario. Car-following phenomena are widely acknowledged as effective models for the observation and simulation of microscopic traffic flow. As illustrated in Figure 3, a car-following pair is composed of the subject vehicle and the vehicle leading it. In this context, v_i, Δv, and Δx denote the speed of the subject vehicle, the speed difference, and the gap distance, respectively. Consequently, a car-following model serves to illustrate the interactions between adjacent vehicles. The primary objective of a car-following model is to predict the speeds of the subject vehicle based on these crucial parameters.

2.4. Transformer-Enhanced Deep Learning Model for Speed Prediction. Deep learning techniques have gained significant popularity, leading to the emergence of numerous data-driven approaches that exhibit greater fidelity and robustness compared to conventional methods [46]. The attention mechanism and Transformer module, innovative architectures in the field of deep learning, have inspired research in computer vision and natural language processing since their introduction in 2017 [47]. The Transformer module typically combines an Encoder-Decoder structure with an improved self-attention mechanism. Recently, the application of the Transformer module to time-sequence forecasting problems [48, 49] has shown superior performance compared to other sequence models.

As shown in Figure 4(a), the self-attention mechanism is realized through the scaled dot-product operation. Initially, the input sequence, denoted as $\mathbf{X}$, is mapped into three vectors: the query vector $\mathbf{Q}$, key vector $\mathbf{K}$, and value vector $\mathbf{V}$. This mapping is computed as per the following equation:

$$\begin{aligned}\mathbf{Q} &= \mathbf{X}\mathbf{W}^{(\mathbf{Q})},\\ \mathbf{K} &= \mathbf{X}\mathbf{W}^{(\mathbf{K})},\\ \mathbf{V} &= \mathbf{X}\mathbf{W}^{(\mathbf{V})},\end{aligned} \tag{1}$$

where $\mathbf{X} \in \mathbb{R}^{T\times d_x}$, $\mathbf{W}^{(\mathbf{Q})} \in \mathbb{R}^{d_x\times d_k}$, $\mathbf{W}^{(\mathbf{K})} \in \mathbb{R}^{d_x\times d_k}$, and $\mathbf{W}^{(\mathbf{V})} \in \mathbb{R}^{d_x\times d_v}$ are linear matrices. Here, T and d_x denote the length and dimensions of $\mathbf{X}$, respectively, while d_k, d_k, and d_v represent the dimensions of $\mathbf{Q}$, $\mathbf{K}$, and $\mathbf{V}$, respectively.

Further, as per equation (2), $\mathbf{Q}$ and $\mathbf{K}$ are aggregated using the dot-product operation. The resultant values are then normalized by the scale factor $\sqrt{d_k}$ and subjected to the

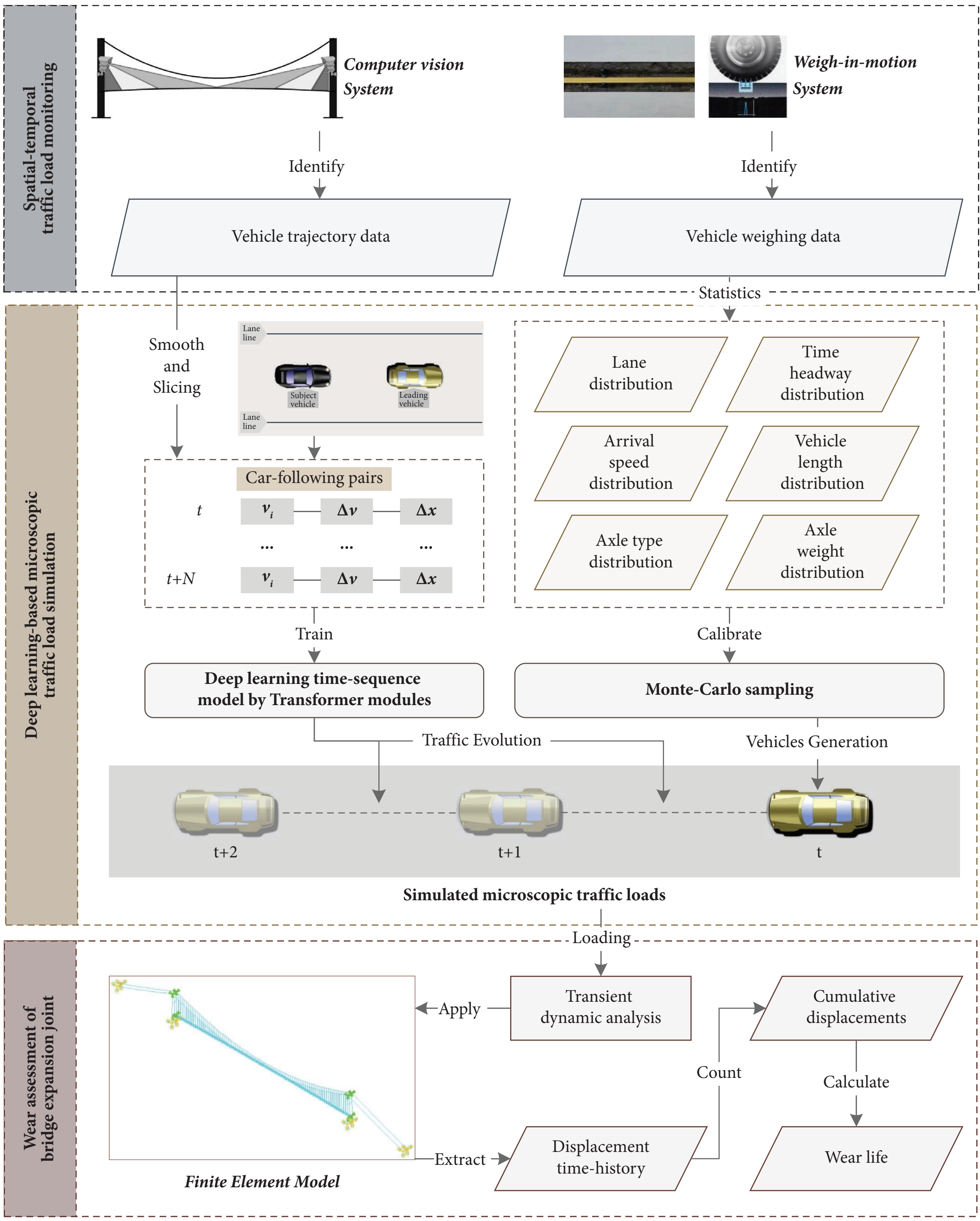

Figure 1: Overview of Transformer-enhanced TLS for wear evaluation of BEJs.

Softmax operation. Ultimately, the outcome is multiplied by $\mathbf{V}$ to yield the final output vector $\mathbf{Z}$.

$$\begin{aligned}\mathbf{Z} &= \text{Attention}(\mathbf{Q}, \mathbf{K}, \mathbf{V}) \\ &= \text{Softmax}\left(\frac{\mathbf{Q}\mathbf{K}^T}{\sqrt{d_k}}\right)\mathbf{V}.\end{aligned} \tag{2}$$

In their work [47], Vaswani discovered the benefits of linearly projecting vectors of varying dimensions, which led to the proposition of the multihead self-attention (MHSA) approach, as illustrated in Figure 4(b). MHSA allows the model to attend to information from different representation subspaces at diverse positions simultaneously. Consequently, MHSA constitutes a critical component of the Transformer layer, as defined by the following equation:

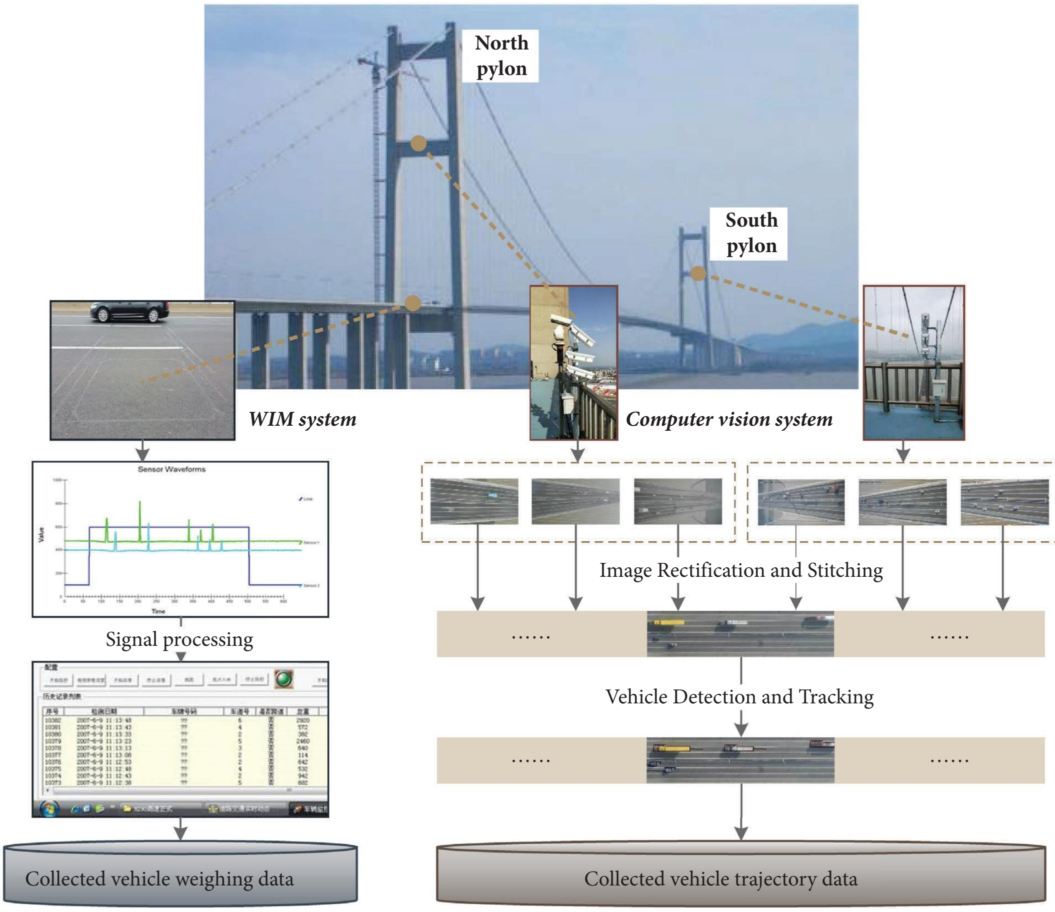

FIGURE 2: Full-span spatial-temporal traffic load acquisition [44, 45].

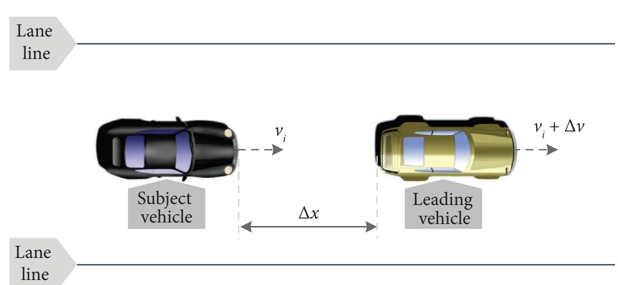

FIGURE 3: A car-following pair in the microscopic TLS scenario.

$$\mathbf{Z_i} = \text{Softmax}\left(\frac{\mathbf{Q_i}\mathbf{K_i}^T}{\sqrt{d_k}}\right)\mathbf{V_i},$$
$$\text{MultiHead}(\mathbf{Q},\mathbf{K},\mathbf{V}) = \text{Concat}(\mathbf{Z_1},\mathbf{Z_2},\ldots,\mathbf{Z_h})\mathbf{W^O}, \tag{3}$$

where h denotes the number of heads. All $\mathbf{W}$ are linear weight matrices that are learned from the data.

In this study, we specifically employ Transformer modules for the time-sequence speed prediction of each vehicle traversing the bridge deck, thereby achieving the traffic evolution prediction within the TLS procedure. As depicted in Figure 5, the input sequences are time series data of three key parameters derived from the car-following pair data, namely, $(v_i, \Delta v, \Delta x)$. The dimension of the input sequence is $3 \times T$, where T denotes the number of historical data steps.

These vectors are subsequently passed through the Encoder-Decoder structure, which is composed of N stacked Transformer modules and feed-forward layers. Here N represents the number of identical layers that constitute the Encoder and Decoder. Following this, a fully connected layer is applied to generate the final output. The dimension of this output sequence is $1 \times L$, where L denotes the number of predicted steps. Consequently, the Transformer-enhanced model maps the input sequence to the output sequence, as demonstrated in the following equation:

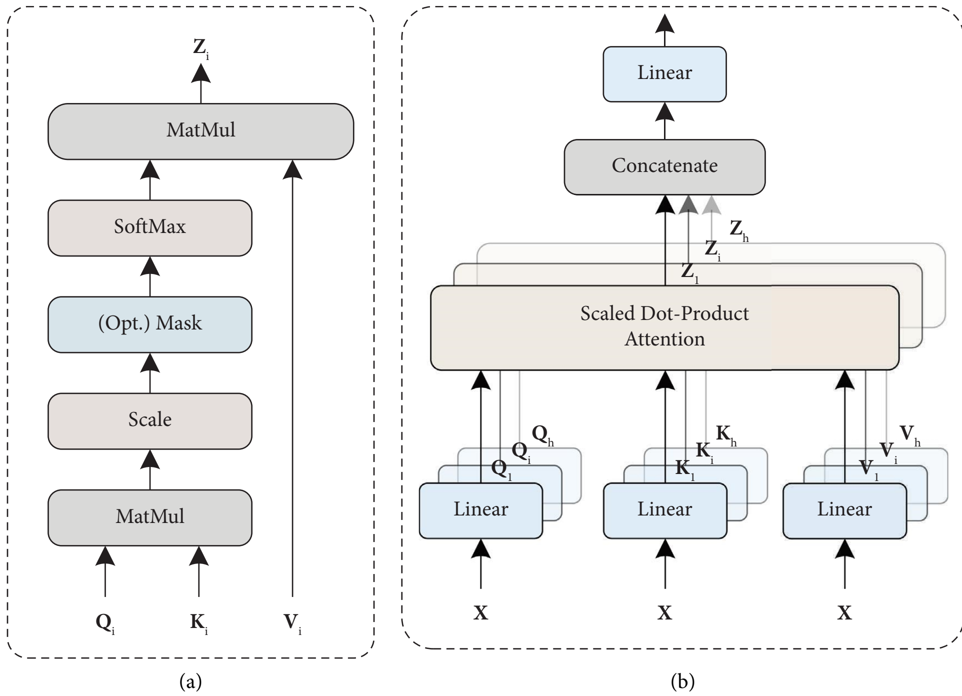

Figure 4: Attention mechanism in the Transformer module. (a) Scaled dot-product attention. (b) Multihead attention.

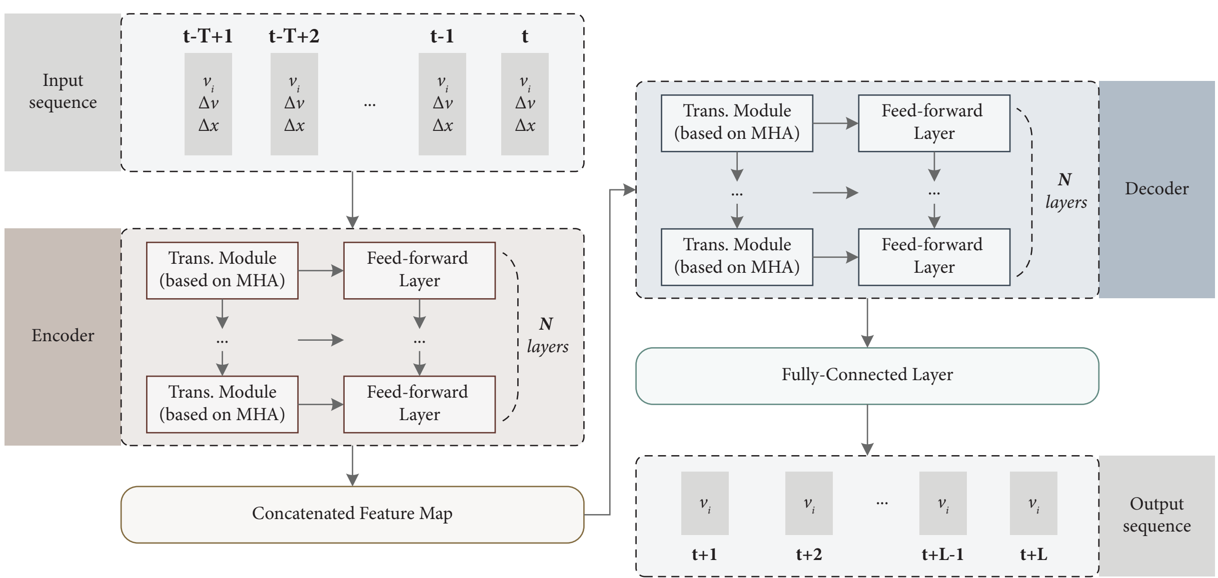

Figure 5: Transformer-enhanced deep learning model for speed prediction.

$$\left(v_i(t+1),\ldots,v_i(t+L)\right) = \text{Model}\begin{pmatrix} v_i(t-T+1),\ldots,v_i(t) \\ \Delta v(t-T+1),\ldots,\Delta v(t) \\ \Delta x(t-T+1),\ldots,\Delta x(t) \end{pmatrix}. \tag{4}$$

2.5. Transient Dynamic Analysis for Displacement Calculation. The transient dynamic analysis (TDA) approach is required to compute the displacement history of the bridge under traffic loads, utilizing the following dynamic equation:

$$[\mathbf{M}]\{\ddot{\mathbf{u}}\} + [\mathbf{C}]\{\dot{\mathbf{u}}\} + [\mathbf{K}]\{\mathbf{u}\} = \{\mathbf{F}(t)\}, \tag{5}$$

where $[\mathbf{M}]$ represents the mass matrix, $[\mathbf{C}]$ denotes the damping matrix, $[\mathbf{K}]$ signifies the stiffness matrix, $\ddot{\mathbf{u}}$ is the node acceleration vector, $\dot{\mathbf{u}}$ is the node velocity vector, $\mathbf{u}$ is the node displacement vector, and $\mathbf{F}(t)$ is the dynamic load vector.

The direct integration method, based on the Newmark-β method proposed by Newmark in 1959, is an efficient approach to solving the dynamic equation. This method utilizes the following iterative formulas:

$$\begin{aligned}\dot{\mathbf{u}}_{i+1} &= \dot{\mathbf{u}}_i + [(1-\gamma)\Delta t]\ddot{\mathbf{u}}_i + (\gamma\Delta t)\ddot{\mathbf{u}}_{i+1},\\ \mathbf{u}_{i+1} &= \mathbf{u}_i + (\Delta t)\dot{\mathbf{u}}_i + \left[(0.5-\beta)(\Delta t)^2\right]\ddot{\mathbf{u}}_i + \left[\beta(\Delta t)^2\right]\ddot{\mathbf{u}}_{i+1},\end{aligned} \tag{6}$$

where β and γ are integration constants that determine the method's precision and stability. The Newmark-β method remains stable if the time step satisfies the following condition:

$$\frac{\Delta t}{T_n} \leq \frac{1}{\pi\sqrt{2}}\frac{1}{\sqrt{\gamma-2\beta}}. \tag{7}$$

Continuing to rearrange equation (6), we obtain

$$\begin{aligned}\ddot{\mathbf{u}}_{i+1} &= \frac{1}{\beta(\Delta t)^2}\left(\mathbf{u}_{i+1}-\mathbf{u}_i\right) - \frac{1}{\beta\Delta t}\dot{\mathbf{u}}_i - \left(\frac{1}{2\beta}-1\right)\ddot{\mathbf{u}}_i,\\ \dot{\mathbf{u}}_{i+1} &= \frac{\gamma}{\beta\Delta t}\left(\mathbf{u}_{i+1}-\mathbf{u}_i\right) - \left(\frac{\gamma}{\beta}-1\right)\dot{\mathbf{u}}_i - \frac{\Delta t}{2}\left(\frac{\gamma}{\beta}-2\right)\ddot{\mathbf{u}}_i.\end{aligned} \tag{8}$$

By substituting (8) into (5), we derive an equation that contains only the unknown $\mathbf{u}_{i+1}$, which can be solved to obtain $\mathbf{u}_{i+1}$. Further substituting $\mathbf{u}_{i+1}$ into equation (8), we can determine $\dot{\mathbf{u}}_{i+1}$ and $\ddot{\mathbf{u}}_{i+1}$, thereby accomplishing the computation for a single time step.

To utilize the Newmark-β method for evaluating the wear damage of BEJs, a sequential approach is established. This approach, based on the proposed Transformer-enhanced vehicle speed prediction model and TDA, comprises four major steps:

(i) *Step 1*. Calibrate the Monte Carlo simulators and train the Transformer-enhanced model using observed data. Then, obtain TLS results for the specified time range.

(ii) *Step 2*. Load the TLS results onto the nodes of the FEM according to the loading steps and locations. If there are no nodes at the loading location, distribute the load between the two adjacent nodes in inverse proportion.

(iii) *Step 3*. Import the loading data into the ANSYS software in a step-by-step manner and initiate TDA starting from the first step.

(iv) *Step 4*. Extract the longitudinal displacement of the expansion joint at each step. Then, calculate cumulative displacements to evaluate the wear damage of the BEJ.

3. Experimental Setup

3.1. Bridge Information. An on-site experiment was conducted on the Runyang Suspension Bridge (RSB), a bridge that spans the Yangtze River in China. The RSB is a long-span suspension bridge, featuring a flat steel box girder and two H-shaped reinforced concrete pylons. The bridge includes a central span of 1,490 m, two side spans of 470 m, and two pylons with a height of 207 m. The design incorporates 180 suspenders and 2 central buckles to connect the main cable with the bridge deck. Additionally, the typical cross section of the girder measures 38.7 m in width and 3 m in height. The deck accommodates six standard lanes and two emergency lanes, with widths of 3.75 m and 3 m, respectively. Figure 6 provides a depiction of the overall layout of the RSB.

3.2. Vehicle Trajectory Reconstruction. Upon the installation of the traffic load monitoring system, vehicle trajectory data can be collected across the entire bridge deck at each time point. However, due to factors such as perspective distortion, occlusion, and other imaging inaccuracies, positional measurement errors may arise. These errors can adversely affect the modeling performance of data-driven approaches [50]. To mitigate this, we employ four processing steps to reconstruct the raw speeds captured by the monitoring system, based on previous research by Montanino [51].

Firstly, extreme positional errors, referred to as "outliers," are eliminated by substituting these data points with synthetic ones. Secondly, random noise, which manifests as excessive peaks and valleys, is mitigated by applying a low-pass digital filter. Thirdly, unreasonable local trajectories are examined and reconstructed using the physically consistent rule of the vehicle. Lastly, residual noise is eradicated by reapplying the low-pass filter.

An example of trajectory reconstruction is illustrated in Figure 7(a), with the corresponding accelerations of the vehicle shown in Figure 7(c). Simultaneously, the relative speeds and gaps between the vehicle and its leading vehicle are displayed in Figures 7(b) and 7(d). The reconstructed speeds exhibit enhanced consistency and reasonableness compared to the raw data, thereby contributing to the improved performance of subsequent training of data-driven TLS models.

3.3. Finite Element Modeling and Verification. Upon acquiring the TLS data, a precise FEM of the RSB is required to compute the time-sequence displacements and further evaluate the BEJ. A FEM of the RSB is constructed using ANSYS software, as depicted in Figure 8. Concretely, the Beam4 element type is employed for modeling the girder, pylons, and central buckles. The Link10 element type is used for the main cables and suspenders, while the Mass21 element type represents the weights from the pavements and diaphragms. Lastly, the Combin37 element type is utilized for the BEJs at both ends of the girder.

Specifically, the Combin37 element type is designed to simulate a nonlinear spring with force-speed characteristics, with the damping force calculated using equation (9). Based on prior research [52], we set $c = 3750\ \mathrm{kN}\cdot(\mathrm{m}\cdot\mathrm{s})^{-\alpha}$ and $\alpha = 0.4$.

$$f = c|v|^{\alpha}\operatorname{sgn}(v), \tag{9}$$

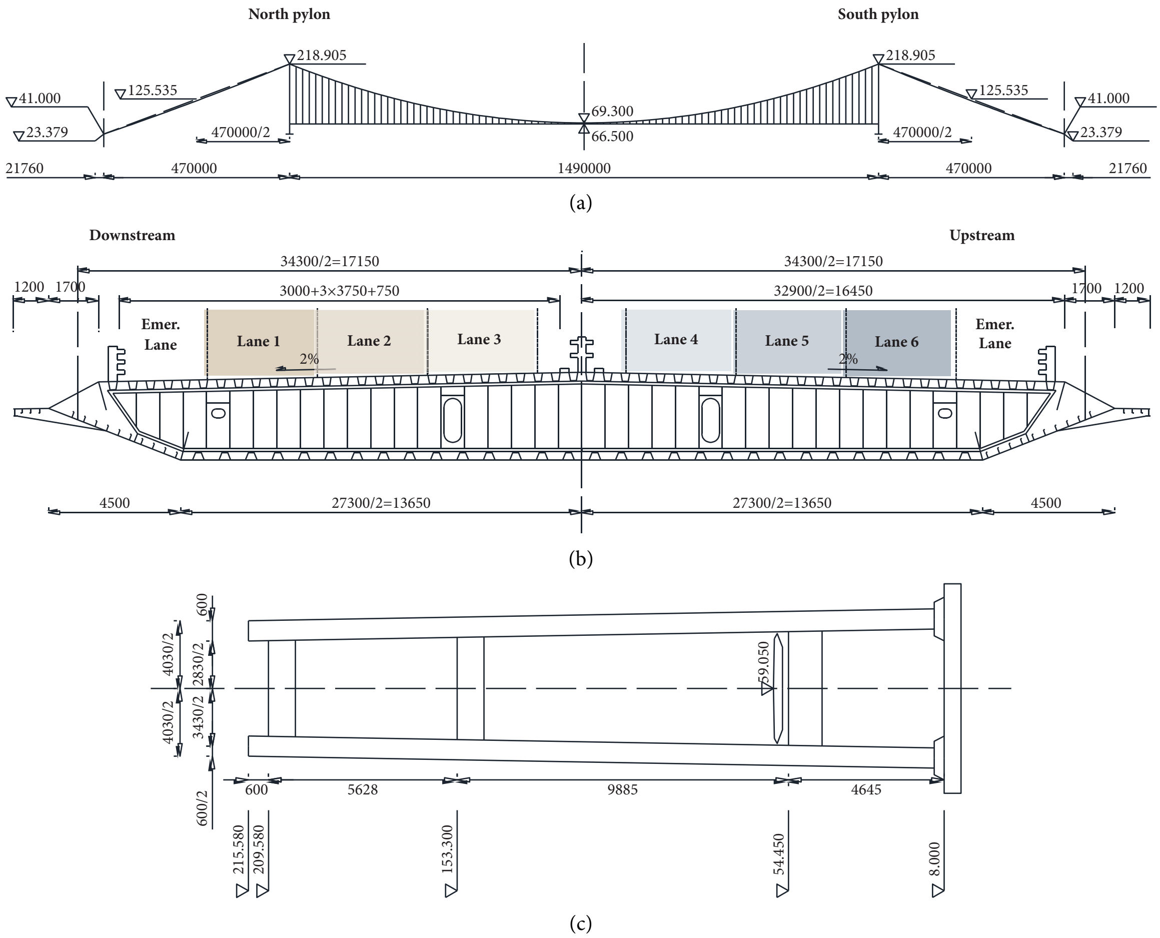

Figure 6: Main configurations of RSB. (a) Elevation view. (b) Cross section of the girder. (c) Pylon.

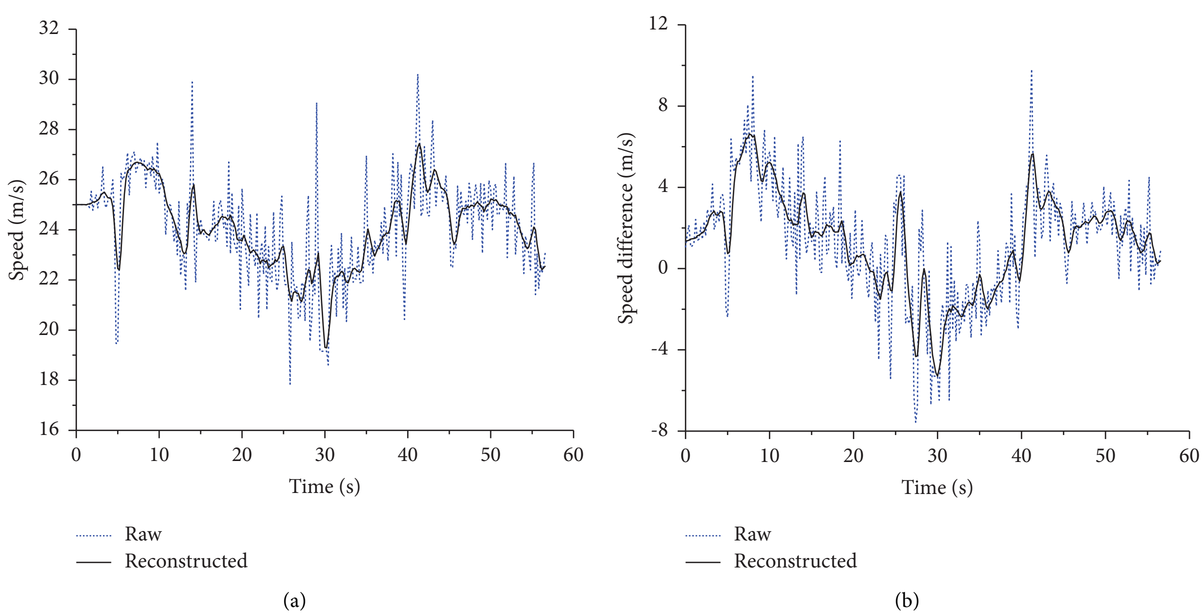

Figure 7: Continued.

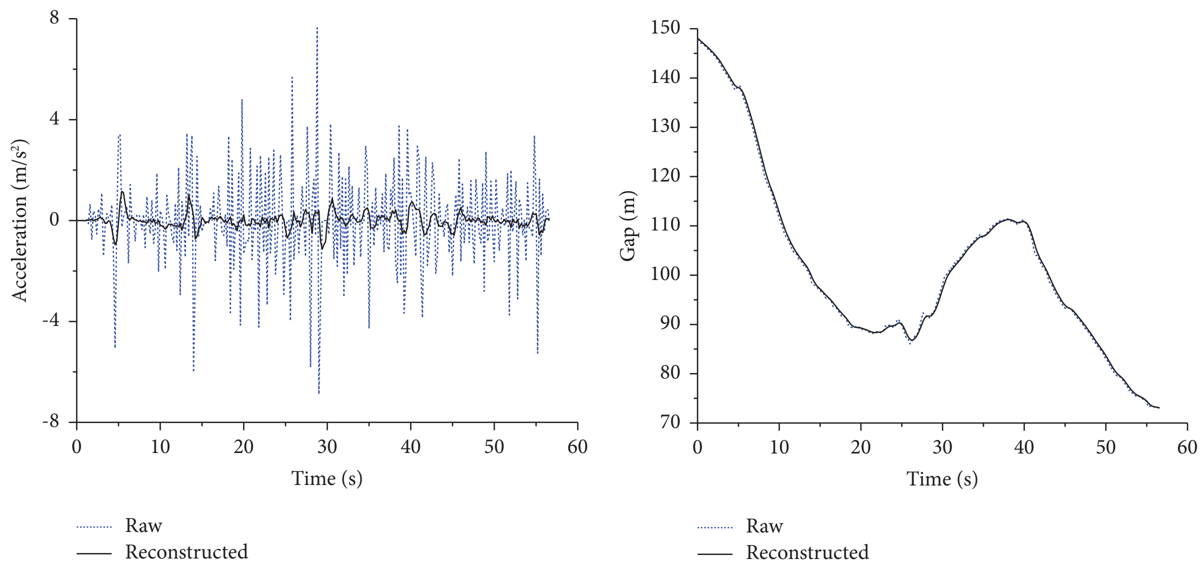

Figure 7: Comparative illustration of raw and reconstructed vehicle trajectory profiles. (a) Speed (v) comparison. (b) Speed difference (Δv) comparison. (c) Acceleration $(\mathrm{d}v/\mathrm{d}t)$ comparison. (d) Gap (Δx) comparison.

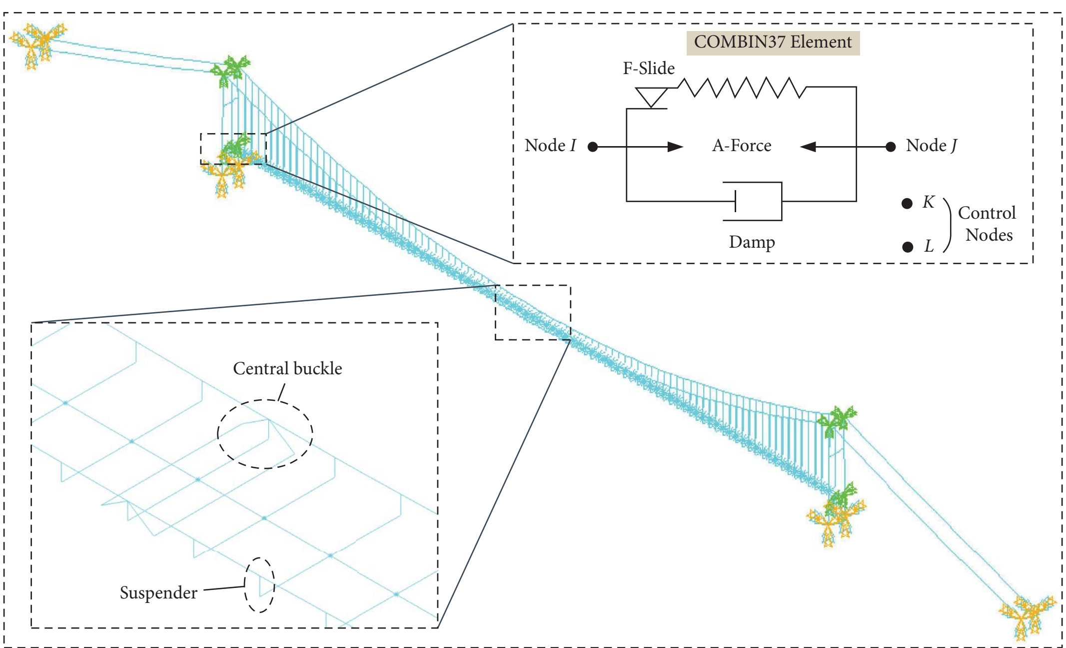

Figure 8: FEM of the RSB.

where c represents the damping factor, α is a constant exponent, sgn is a sign function indicating the direction of the damping force, and v denotes the relative speed between the two nodes of the element.

The FEM of the RSB is validated in both static and dynamic aspects. Initially, the longitudinal stiffness of the FEM is compared with data from an early static test [52]. The static test contains two static loading cases, achieved by positioning 52 identical trucks, each weighing 30.0 t. As listed in Table 1, the longitudinal displacements of BEJs calculated by the FEM align well with those from the static test.

In addition, the dynamic behavior of the established FEM has been computed, with the results presented in Table 2. The in situ testing results from a previous study [53] serve as the measured frequencies for error evaluation. The results indicate that the modal parameters of the FEM align well with the measured values, including both the nature of modes and their corresponding frequencies.

Table 1: Verification of the static behavior of the established FEM.

		Static test (mm)	FEM calculation (mm)	Relative error (%)
1st case	North end	463.10	422.03	−8.9
1st case	South end	472.00	437.81	−7.2
2nd case	North end	10.50	9.40	−10.5
2nd case	South end	7.30	8.29	13.6

Table 2: Verification of the dynamic behavior of the established FEM.

Mode no.	Nature of mode	Measured frequency (Hz)	FEM analysis (Hz)	Error (%)
1	1st symmetric lateral	0.0586	0.0534	−8.9
2	1st anti-symmetric vertical	0.0877	0.0884	0.8
3	1st anti-symmetric lateral	0.1221	0.1228	0.6
4	1st symmetric vertical	0.1587	0.1504	−5.2
5	2nd symmetric vertical	0.1685	0.1668	−1.0
6	2nd anti-symmetric vertical	0.1880	0.1877	−0.2
7	1st symmetric torsional	0.2417	0.2307	−4.6
8	1st anti-symmetric torsional	0.3077	0.2862	−7.0

4. Results and Discussion

4.1. Transformer-Enhanced Model Training and Evaluation. For model training, the PyTorch framework is utilized to conduct all deep learning-based experiments. The experiments are performed on a desktop PC equipped with an Intel® Core(TM) i7-6700k CPU, 32 GB RAM, and an NVIDIA GeForce GTX 1080Ti GPU, with the support of CUDA v10.2 and cuDNN v7.6.5.

In terms of setting training parameters, we set the learning rate to 0.001. The batch size for each update is set to 128, considering memory cost. As speed prediction is a regression problem, the dropout rate is set to 0. The total number of epochs for the training process is initially set to 100, with early stopping of model training occurring if the validation loss does not decrease after 10 epochs. Furthermore, by splitting the car-following pairs, we allocate the training set, validation set, and test set in a ratio of 0.70 : 0.15 : 0.15.

Subsequently, for evaluation, we employ the mean square error (MSE) and mean absolute error (MAE) metrics, defined in equation (10). MSE is used to visualize the trend of loss value during training, while MAE is applied to the test set to evaluate the precision of the model after training.

$$MSE = \frac{1}{N}\sum_{j=1}^{N}\left(\hat{v}_j - v_j\right)^2,$$
$$MAE = \frac{1}{N}\sum_{j=1}^{N}\left|\hat{v}_j - v_j\right|, \tag{10}$$

where N represents the number of samples and $\hat{v}_j$ and v_j denote the predicted and actual speed of the j-th vehicle, respectively.

To optimize the performance of the Transformer-enhanced model, we implement hyperparameter optimization. In this study, we select the number of layers, historical inputs, and predicted outputs for optimization, as they are the primary factors constituting the deep learning model. Thus, training and evaluation are conducted for each combination of hyperparameters, with the results depicted in Figure 9. The final selected parameters are listed below, and the model achieved a minimum MAE of 0.1738 m/s.

(i) N (number of layers): 3
(ii) T (historical inputs): 40
(iii) L (prediction outputs): 18

During the training and evaluation phase, the chosen hyperparameters are utilized to monitor the model's performance. The loss curve, as illustrated in Figure 10, demonstrates a consistent decrease and convergence of loss values for both the training and validation sets. This trend signifies an enhancement in the model's ability to predict speed. Notably, the final loss values for the training and validation sets are remarkably similar, suggesting that the model is not overfitting.

4.2. Comparison of Data-Driven TLS Models

4.2.1. Performance Comparison for Single-Step Prediction. Previous studies have utilized machine learning and deep learning models such as SVM [54], ANN [55], LSTM [56], GRU [57], and Seq2Seq [58] to tackle the time-sequence prediction problem of subject vehicles.

To evaluate the performance of various data-driven models, we conduct a comparison of the prediction errors on the test set between these models and the Transformer-enhanced model. These comparative models are trained on the same training and validation set as the Transformer-enhanced model, with their hyperparameters optimized to ensure the best possible results. The MAE of all models is detailed in Table 3.

As indicated by the table, the Transformer-enhanced model achieves a lower error rate compared to the other

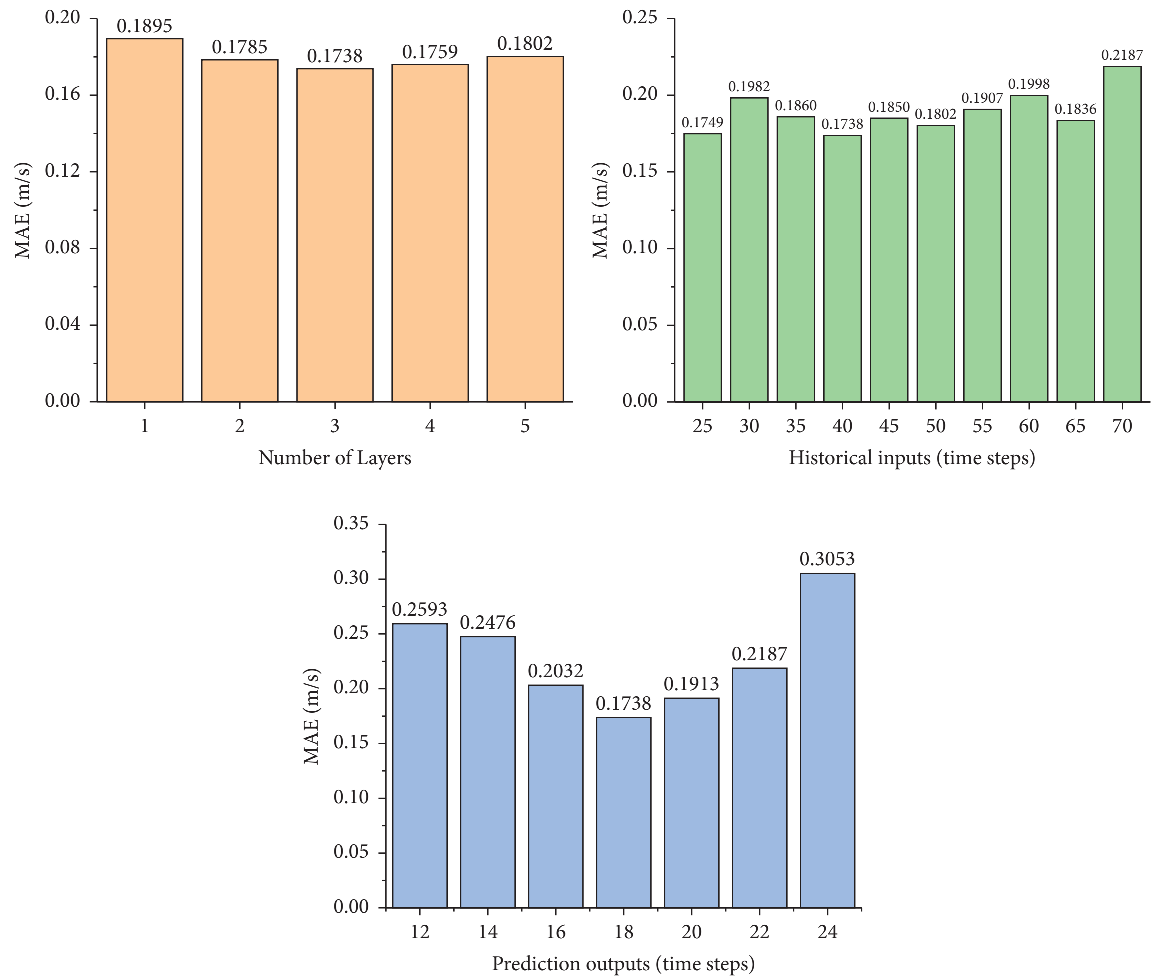

Figure 9: Hyperparameter optimization for the Transformer-enhanced model.

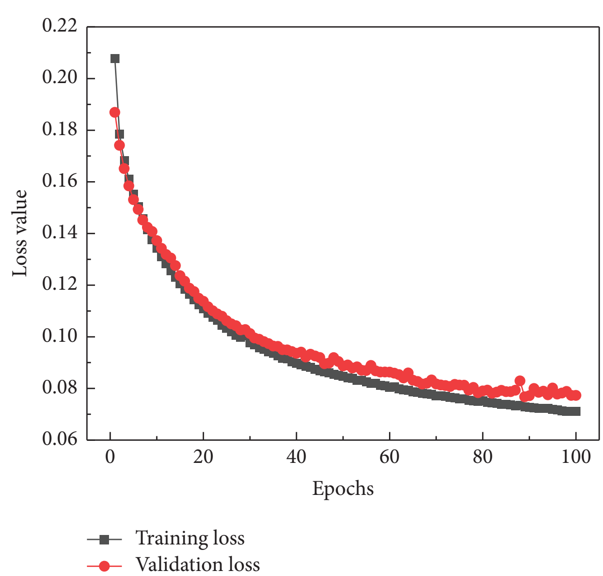

Figure 10: Loss curves of the Transformer-enhanced model during training.

Table 3: Comparative performance of data-driven models for speed prediction.

Model	Detailed information	MAE (m/s)
SVM	Kernel: radial basis function Regularization parameter: 5.0	0.4321
ANN	Nodes in hidden layer #1: 64 Nodes in hidden layer #2: 32	0.3241
LSTM	Nodes in hidden layer #1: 32 Nodes in hidden layer #2: 16	0.2463
GRU	Nodes in hidden layer #1: 32 Nodes in hidden layer #2: 8	0.2316
Seq2Seq with GRU	Encoder GRU: nodes in hidden layer #1: 32, nodes in hidden layer #2: 32 Decoder GRU: nodes in hidden layer #1: 32, nodes in hidden layer #2: 16	0.1961
Transformer	Encoder Transformer layers: 3 Decoder Transformer layers: 3	0.1738

models. Moreover, due to their ability to extract more profound features from sequences, deep learning-based time-sequence models outperform machine learning-based models. At the same time, the Seq2Seq model demonstrates superior performance over the original GRU and LSTM models.

4.2.2. Performance Comparison for Full-Bridge Evolution Prediction. Prior to its application in TLS, the trained Transformer-enhanced model undergoes further validation by comparing its trajectory prediction with the observed data. Specifically, for the tested subject vehicle, the positions of its leading vehicle are maintained identical to the actual observed data. Meanwhile, the speeds of the subject vehicle are predicted by the Transformer-enhanced model at each time step, with the latest vector $(v_i, \Delta v, \Delta x)^T$ being updated after each prediction. Thus, the updated positions of the subject vehicle can be computed recursively by using the following equation:

$$\widehat{x}(t+1) = \widehat{x}(t) + \widehat{v}(t+1)\Delta t + \frac{1}{2}(\widehat{v}(t+1) - \widehat{v}(t))\Delta t^2. \tag{11}$$

The trained deep learning models are employed for predicting the trajectory of each subject vehicle in the test set. Concurrently, the MAE of the vehicle speed at each step for each subject vehicle is calculated and presented in Table 4. The results revealed that the errors of the entire trajectory profiles are larger than the errors of scattered samples from Table 3, considering the cumulative effect. Nevertheless, the trained Transformer-enhanced model outperforms the others and achieves the lowest error at 0.4376 m/s.

To provide a visual representation of the model evaluation process, an example with errors similar to the MAE in Table 4 is selected. As a result, the trajectory profile of vehicle ID 1401 is chosen and depicted in Figure 11, which includes the speed, speed difference, acceleration, and gap curves of the car-following pair. As observed from Figures 11(a), 11(b), and 11(d), all trained deep learning models are capable of reconstructing the time-sequence trends of the subject vehicle. Furthermore, by examining the acceleration

Table 4: Performance comparison of deep learning models for full-bridge trajectory prediction.

Model	MAE (m/s)
LSTM	1.4089
GRU	0.8069
Seq2Seq with GRU	0.6395
Transformer	0.4376

values in Figure 11(c), it is evident that the Seq2Seq and Transformer-enhanced models exhibit less oscillation than the LSTM and GRU models. The Transformer-enhanced model provides a smoother and more consistent output with the observed data compared to other models.

4.3. TLS Based on Transformer-Enhanced Model and Monte Carlo Sampling. Figure 1 illustrates the process following the calibration of the Monte Carlo simulators and the training of the Transformer-enhanced model, which enables the implementation of the microscopic TLS for subsequent applications.

In this study, a one-hour TLS is conducted, producing spatial-temporal traffic load data for the entire bridge. Specifically, the Monte Carlo simulators generate vehicles for each lane through random sampling, based on statistical features extracted from the WIM data. The Transformer-enhanced model then predicts the speeds of each generated vehicle in a step-by-step manner until they eventually exit the bridge deck.

Figure 12 displays three frames of the simulated traffic loads, with the gross weights of the vehicles indicated for better understanding. The traffic loads consist of all car-following pairs across the entire bridge deck. The proposed TLS has demonstrated its capability for high-precision modeling and simulation of the actual observed traffic load flow. For instance, the pair highlighted in the blue box accurately emulates the deceleration behavior of the subject vehicle.

In addition to the microscopic behaviors of car-following pairs, the macroscopic characteristics of the TLS method have been validated through a comparison of vehicle speeds derived from the TLS data and the observed data. For

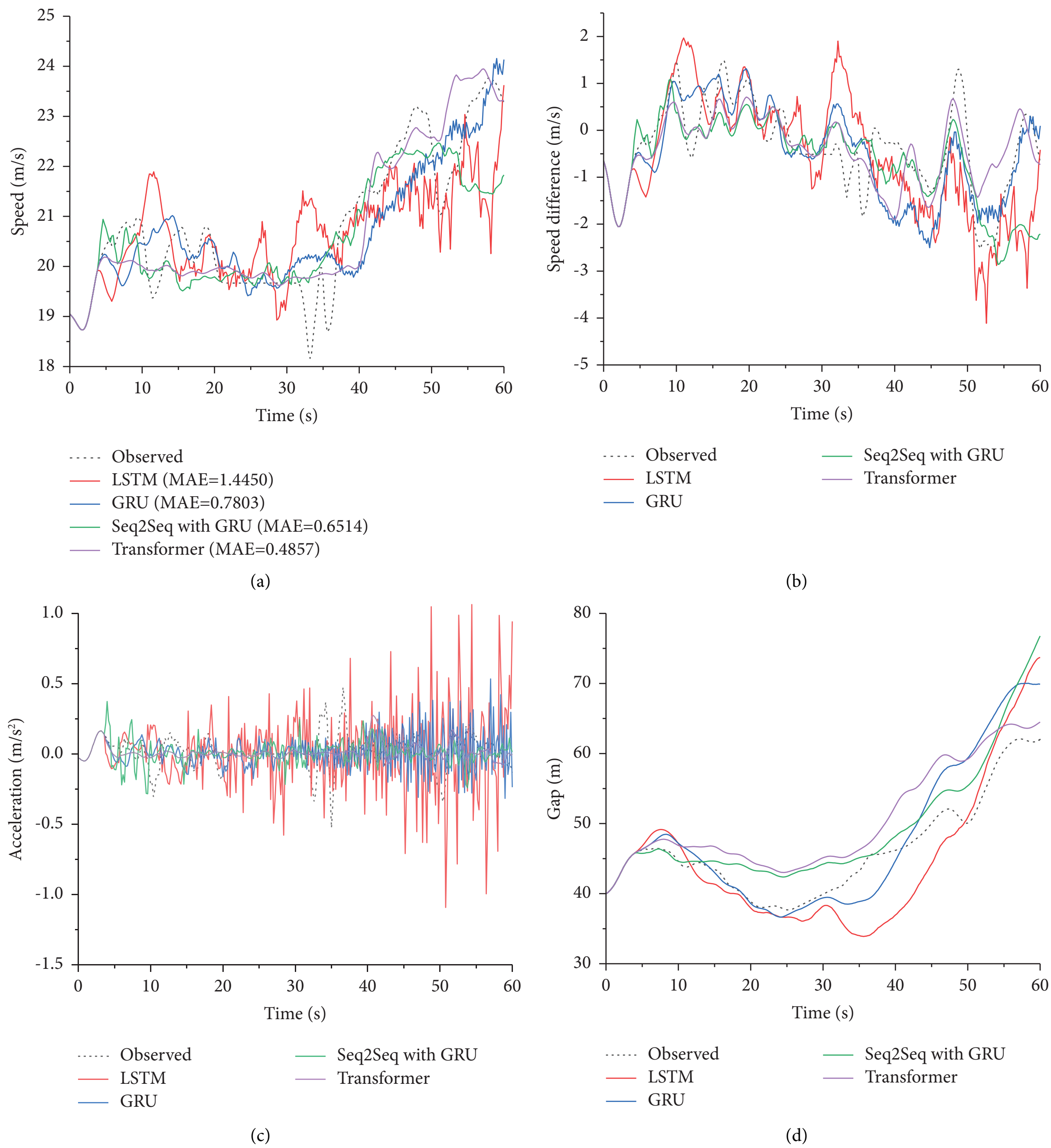

FIGURE 11: Trajectory profile of vehicle-1401. (a) Speed (v) curves. (b) Speed difference (Δv) curves. (c) Acceleration $(\mathrm{d}v/\mathrm{d}t)$ curves. (d) Gap (Δx) curves.

a more quantitative analysis, we calculated the 25%, 50%, and 75% quantile values of vehicle speeds, which are detailed in Table 5. Overall, the vehicle speeds generated by the TLS method show a strong alignment with the observed data, especially in Lane #3, where the errors are less than 4%. The maximum error observed is 11.1% of the 25% quantile value in Lane #5. Considering the significantly lower number of vehicles and samples in Lane #5 used for model training compared to Lane #3, it is expected that these errors could be substantially minimized by enlarging the dataset in future studies.

4.4. Cumulative Displacements and Wear Damage Evaluation of BEJ. The simulated one-hour traffic load simulation (TLS) data are incorporated into the established finite element model (FEM) with a time step of 0.1 s. By adhering to the proposed four-step procedure, the time histories of bridge expansion joint (BEJ) displacement are computed and illustrated in Figure 13. Subsequently, the cumulative displacement of the BEJ is determined, yielding a value of 3.684 m for the simulated case. In reference to the critical value of cumulative displacement of the polytetrafluoroethylene (PTFE) plate, the wear life of an intact PTFE plate S

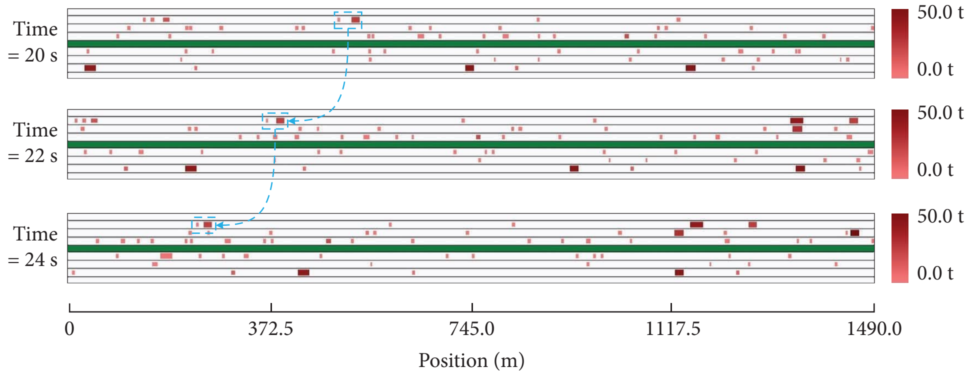

FIGURE 12: TLS on the entire bridge deck.

TABLE 5: Quantitative comparison of speed distribution between TLS data and observed data.

Lane	Item	25% quantile value	50% quantile value	75% quantile value
	Observed data (m/s)	15.87	18.23	20.45
1	TLS data (m/s)	16.33	18.59	20.27
	Relative error (%)	2.9%	2.0%	−0.9%
	Observed data (m/s)	19.20	21.91	24.60
2	TLS data (m/s)	18.01	20.54	22.89
	Relative error (%)	−6.2%	−6.3%	−6.9%
	Observed data (m/s)	22.45	24.42	26.31
3	TLS data (m/s)	21.64	24.69	26.28
	Relative error (%)	−3.6%	1.1%	−0.1%
	Observed data (m/s)	22.07	23.87	25.61
4	TLS data (m/s)	21.38	22.35	23.97
	Relative error (%)	−3.1%	−6.4%	−6.4%
	Observed data (m/s)	19.39	21.83	24.02
5	TLS data (m/s)	17.24	20.01	22.48
	Relative error (%)	−11.1%	−8.4%	−6.4%
	Observed data (m/s)	14.99	17.07	19.50
6	TLS data (m/s)	14.94	16.25	17.86
	Relative error (%)	−0.3%	−4.8%	−8.4%

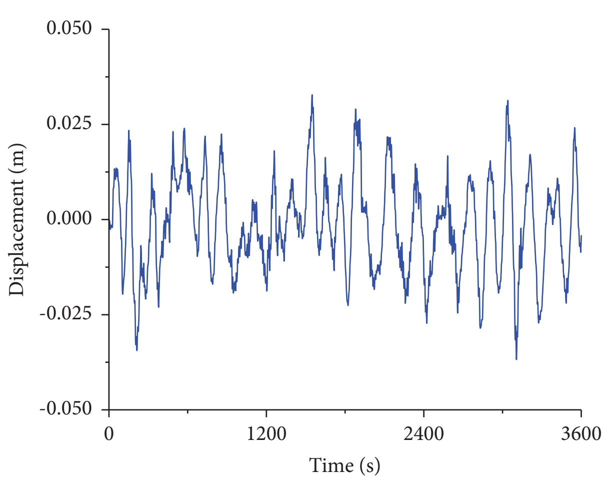

FIGURE 13: BEJ displacement time-histories.

is designed to be 133 km [8]. By applying the cumulative damage rule, the wear damage incurred during this hour can be quantified as 0.0028%.

Furthermore, 24-hour TLS and FEM loading are performed, based on the recorded traffic volume of the RSB on a specific day [59]. The hourly traffic weight is also documented, as shown in Figure 14(a). It can be observed that the trend of cumulative displacement of the BEJ and the hourly traffic weight are highly consistent, both exhibiting peak values during morning and evening rush hours and low values during the early morning off-peak hours. The hourly cumulative wear damage curve is also illustrated in Figure 14(b). It is evident that, considering this traffic load flow as the average level, the PTFE plate of the BEJ has a typical usage time of $1/(6.48571 \times 10^{-4}) = 1542$ days.

4.5. Relationship Analysis between Traffic Weight and Cumulative Displacement. While the TDA based on TLS and FEM offers an accurate evaluation of the wear performance of the BEJ, this procedure can be time-intensive. For more predictive and effective maintenance of BEJs, it is essential to examine the relationships between cumulative displacement and key parameters, necessitating a simplified surrogate model designed for engineering applications.

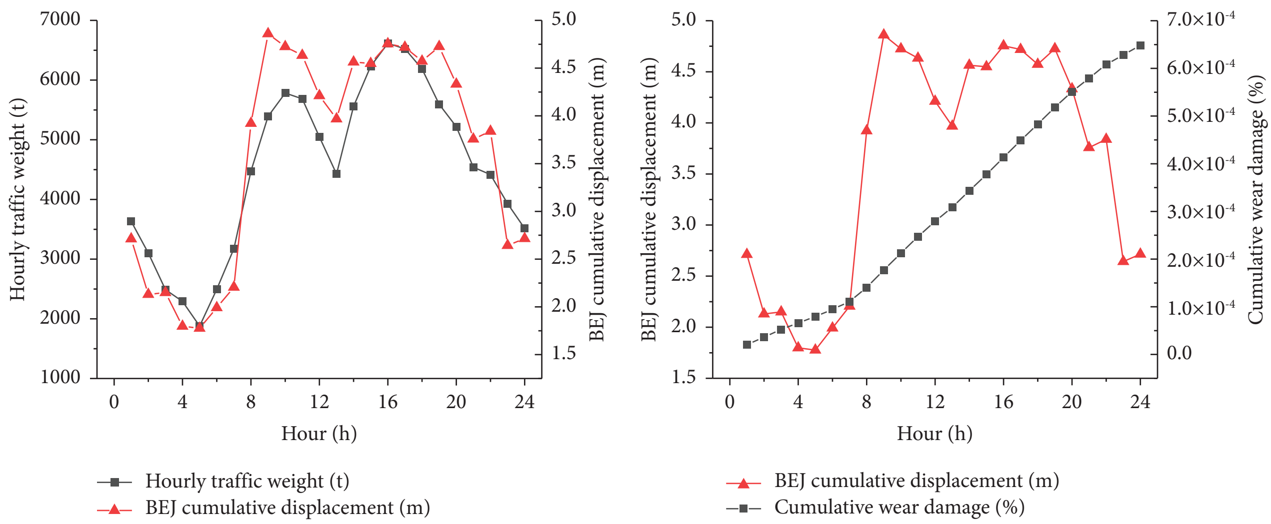

(a) (b)

FIGURE 14: 24-hour analysis of cumulative displacement and wear damage of BEJ. (a) Hourly traffic weight and cumulative displacement. (b) Cumulative wear damage by cumulative displacement.

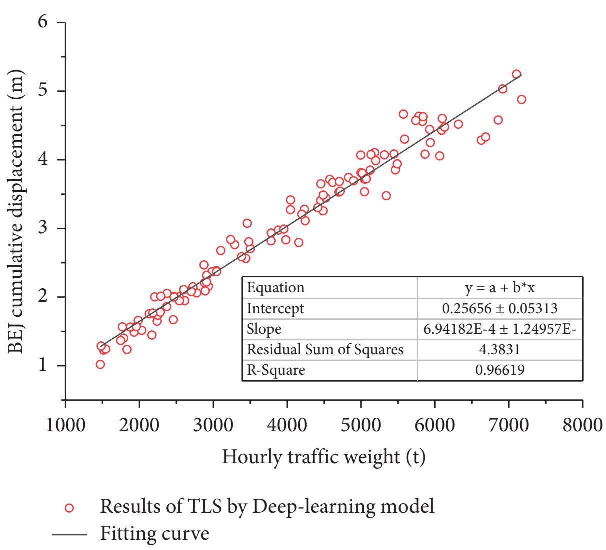

FIGURE 15: Relationship between hourly traffic weight and BEJ cumulative displacement (traffic evolution by deep learning).

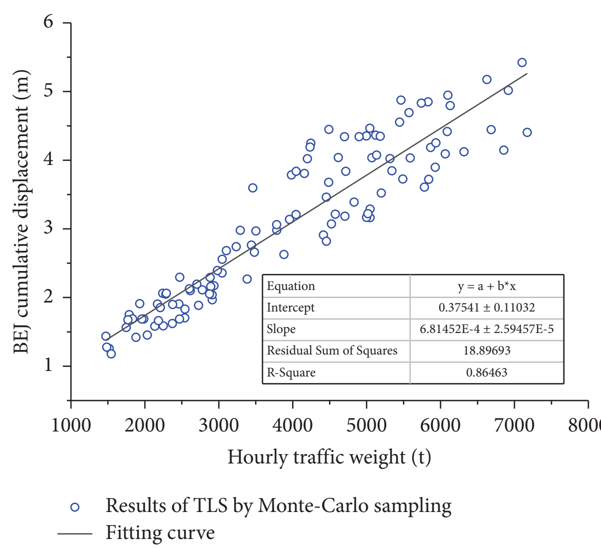

FIGURE 16: Relationship between hourly traffic weight and BEJ cumulative displacement (traffic evolution by consistent-speed assumption).

Consequently, we conduct hundreds of simulations with varying traffic volumes. Specifically, Monte Carlo sampling and the Transformer-enhanced deep learning model are utilized for vehicle generation and traffic evolution prediction, respectively, as depicted in Figure 1. Cumulative displacements of the BEJ are then obtained through comprehensive TDA. The scatter plot, displayed in Figure 15, reveals a robust linear relationship between the two variables. The goodness of fit for the linear model, represented by R-squared, achieved a value of $R^2 = 0.96619$. This fitted model can act as an accurate surrogate model, facilitating rapid evaluation of BEJs' long-term performance in real-world engineering scenarios.

Conventionally, only Monte Carlo sampling is employed in the TLS procedure, which assumes that the generated vehicles move at a uniform speed along the road centerline to form TLS results. This method has been widely applied in previous studies [8, 21]. For comparison purposes, we also implemented an experiment involving hundreds of simulations based on this method. The results are shown in the scatter plot in Figure 16, indicating that the linear relationship still holds. However, the goodness of fit for the model is $R^2 = 0.86463$, and the slope is less than that of the surrogate model obtained from the deep learning model proposed in this paper.

In conclusion, our proposed Transformer-enhanced deep learning model takes into account the interactions between vehicles, thereby reflecting the actual spatial-temporal traffic load with high fidelity. Therefore, the surrogate model based on our proposed Transformer-enhanced method outperforms the conventional Monte Carlo sampling method with a consistent speed assumption and exhibits more conservative damage results in this study.

5. Conclusions

High-fidelity TLS is crucial for the precise evaluation of BEJs and other components of long-span bridges. This study introduces a novel methodology for a more accurate evaluation of BEJ wear due to traffic loads, employing a deep learning-based TLS approach. A deep learning time-sequence model, constructed using Transformer modules, is designed to predict microscopic traffic evolution, thus generating high-accuracy traffic loads on the bridge deck for wear evaluation. Subsequently, the cumulative displacements of BEJs are determined through FEM loading, facilitating the assessment of BEJ wear damage. Additionally, an experimental investigation on an in situ bridge has been conducted, leading to the following conclusions:

(1) By utilizing a large-field traffic load monitoring system, we gathered comprehensive bridge traffic load data and reconstructed vehicle trajectories, thereby minimizing systematic measurement inaccuracies. As a result, a custom benchmark dataset for traffic load evolution was created for the first time.

(2) A deep learning model incorporating the attention mechanism and Transformer modules is developed. This time-sequenced model predicts the speed histories of a vehicle in traffic flow, enabling the prediction of the entire traffic evolution in TLS. The trained model achieved an MAE of 0.1738 m/s and 0.4376 m/s for single-instance and full-bridge speed prediction, respectively. The performance of our model surpasses previous models such as GRU [57], LSTM [39, 40], and Seq2Seq [42].

(3) Our model was integrated with a Monte Carlo sampling simulator for vehicle generation, establishing a TLS method for high-fidelity spatial-temporal traffic loading. Transient dynamic analysis was utilized to derive accurate time histories of BEJ displacement. The cumulative displacement over 24 hours was computed as 6.48571×10^{-4}. Subsequently, a surrogate model was fitted to represent the linear relationship between hourly traffic weight and cumulative displacement. This model achieved an R-squared value of 0.96619, indicating superior performance compared to previous methods, which had an R-squared value of 0.86463.

The methodology proposed in this study provides a comprehensive and precise approach for evaluating the wear of BEJs. Looking ahead, our future work will focus on expanding the TLS dataset to encompass a variety of environmental and traffic conditions. We also plan to make this dataset publicly accessible to facilitate further research in this field. Additionally, we aim to further enhance the accuracy of the deep learning TLS method for the performance evaluation of other bridge components, such as suspenders and cables.

Data Availability

The data used to support the findings of this study can be obtained from the corresponding author upon request.

Conflicts of Interest

The authors declare that they have no conflicts of interest.

Acknowledgments

This work was financially supported by the National Natural Science Foundation of China (grant nos. 52208198, 52238005, 52192663, and 51978514), National Key Research and Development Program of China (grant no. 2021YFF0501004), and Fundamental Research Funds for the Central Universities (grant no. 22120230569).

References

[1] J. Marques Lima and J. de Brito, “Inspection survey of 150 expansion joints in road bridges,” *Engineering Structures*, vol. 31, no. 5, pp. 1077–1084, 2009.

[2] L. M. Chang and Y. J. Lee, “Evaluation of performance of bridge deck expansion joints,” *Journal of Performance of Constructed Facilities*, vol. 16, no. 1, pp. 3–9, 2002.

[3] T. Guo, J. Liu, and L. Y. Huang, “Investigation and control of excessive cumulative girder movements of long-span steel suspension bridges,” *Engineering Structures*, vol. 125, pp. 217–226, 2016.

[4] J. H. Hu, L. H. Wang, X. P. Song, Z. H. Sun, J. F. Cui, and G. P. Huang, “Field monitoring and response characteristics of longitudinal movements of expansion joints in long-span suspension bridges,” *Measurement*, vol. 162, Article ID 107933, 2020.

[5] G. M. Wu, D. H. Yang, T. H. Yi, H. N. Li, and H. Liu, “Sliding life prediction of sliding bearings using dynamic monitoring data of bridges,” *Structural Control and Health Monitoring*, vol. 27, no. 5, 2020.

[6] X. Xu, M. C. Forde, A. Caballero, Y. Ren, and Q. Huang, “Cost-effective maintenance policy for sliding surfaces of bridge bearings using a gamma stochastic process for forecasting,” *Structural Control and Health Monitoring*, vol. 2023, Article ID 5751636, 15 pages, 2023.

[7] Y. Q. Ni, X. G. Hua, K. Y. Wong, and J. M. Ko, “Assessment of bridge expansion joints using long-term displacement and temperature measurement,” *Journal of Performance of Constructed Facilities*, vol. 21, no. 2, pp. 143–151, 2007.

[8] T. Guo, J. Liu, Y. F. Zhang, and S. J. Pan, “Displacement monitoring and analysis of expansion joints of long-span steel bridges with viscous dampers,” *Journal of Bridge Engineering*, vol. 20, no. 9, Article ID 04014099, 2015.

[9] Q. Xia, J. Zhang, Y. D. Tian, and Y. F. Zhang, “Experimental study of thermal effects on a long-span suspension bridge,” *Journal of Bridge Engineering*, vol. 22, no. 7, Article ID 04017034, 2017.

[10] Q. Xia, Y. Xia, H. P. Wan, J. Zhang, and W. X. Ren, “Condition analysis of expansion joints of a long-span suspension bridge through metamodel-based model updating considering thermal effect,” *Structural Control and Health Monitoring*, vol. 27, no. 5, 2020.

[11] C. Q. Miao, Y. Deng, Y. L. Ding, and A. Q. Li, “Damage alarming for bridge expansion joints using novelty detection

technique based on long-term monitoring data," *Journal of Central South University*, vol. 20, no. 1, pp. 226–235, 2013.

[12] R. B. Malla, M. R. Shrestha, M. T. Shaw, and S. B. Brijmohan, "Temperature aging, compression recovery, creep, and weathering of a foam silicone sealant for bridge expansion joints," *Journal of Materials in Civil Engineering*, vol. 23, no. 3, pp. 287–297, 2011.

[13] E. McCarthy, T. Wright, J. E. Padgett, R. DesRoches, and P. Bradford, "Development of an experimentally validated analytical model for modular bridge expansion joint behavior," *Journal of Bridge Engineering*, vol. 19, no. 2, pp. 235–244, 2014.

[14] P. Di Mascio, G. Loprencipe, L. Moretti, L. Puzzo, and P. Zoccali, "Bridge expansion joint in road transition curve: effects assessment on heavy vehicles," *Applied Sciences*, vol. 7, no. 6, p. 599, 2017.

[15] Z. Sun, Z. L. Zou, and Y. F. Zhang, "Utilization of structural health monitoring in long-span bridges: case studies," *Structural Control and Health Monitoring*, vol. 24, no. 10, p. e1979, 2017.

[16] Y. Q. Ni, Y. W. Wang, and C. Zhang, "A bayesian approach for condition assessment and damage alarm of bridge expansion joints using long-term structural health monitoring data," *Engineering Structures*, vol. 212, Article ID 110520, 2020.

[17] Y. M. Zhang, H. Wang, Y. Bai, J. X. Mao, X. Y. Chang, and L. B. Wang, "Switching bayesian dynamic linear model for condition assessment of bridge expansion joints using structural health monitoring data," *Mechanical Systems and Signal Processing*, vol. 160, Article ID 107879, 2021.

[18] Z. H. Chen, X. W. Liu, G. D. Zhou, H. Liu, and Y. X. Fu, "Damage detection for expansion joints of a combined highway and railway bridge based on long-term monitoring data," *Journal of Performance of Constructed Facilities*, vol. 35, no. 4, Article ID 04021037, 2021.

[19] Z. Sun, M. J. Sun, D. M. Siringoringo, Y. Dong, and X. M. Lei, "Predicting bridge longitudinal displacement from monitored operational loads with hierarchical cnn for condition assessment," *Mechanical Systems and Signal Processing*, vol. 200, Article ID 110623, 2023.

[20] Z. W. Wang, X. F. Lu, W. M. Zhang, V. C. Fragkoulis, M. Beer, and Y. F. Zhang, "Deep learning-based reconstruction of missing long-term girder-end displacement data for suspension bridge health monitoring," *Computers & Structures*, vol. 284, Article ID 107070, 2023.

[21] G. L. Li, W. S. Han, X. Chen, T. Guo, Q. Xie, and Y. G. Yuan, "Wear evaluation on slide bearings in expansion joints based on cumulative displacement for long-span suspension bridge under monitored traffic flow," *Journal of Performance of Constructed Facilities*, vol. 34, no. 1, Article ID 04019106, 2020.

[22] A. O'Connor and E. J. O'Brien, "Traffic load modelling and factors influencing the accuracy of predicted extremes," *Canadian Journal of Civil Engineering*, vol. 32, no. 1, pp. 270–278, 2005.

[23] A. Getachew and E. J. Obrien, "Simplified site-specific traffic load models for bridge assessment," *Structure and infrastructure engineering*, vol. 3, no. 4, pp. 303–311, 2007.

[24] B. Enright and E. J. O'Brien, "Monte Carlo simulation of extreme traffic loading on short and medium span bridges," *Structure and infrastructure engineering*, vol. 9, no. 12, pp. 1267–1282, 2013.

[25] S. Pérez Sifre and R. Lenner, "Bridge assessment reduction factors based on Monte Carlo routine with copulas," *Engineering Structures*, vol. 198, Article ID 109530, 2019.

[26] R. F. Gao, J. R. He, and Z. H. Nie, "Stochastic harmonic function-based traffic load simulation method for fatigue damage assessment of concrete bridges," *Probabilistic Engineering Mechanics*, vol. 69, Article ID 103308, 2022.

[27] Z. Sun and X. W. Ye, "Incorporating site-specific weigh-in-motion data into fatigue life assessment of expansion joints under dynamic vehicle load," *Engineering Structures*, vol. 255, Article ID 113941, 2022.

[28] J. Y. Zhou, T. Li, X. J. Ye, and X. F. Shi, "Safety assessment of widened bridges considering uneven multilane traffic-load modeling: case study in China," *Journal of Bridge Engineering*, vol. 25, no. 9, Article ID 05020008, 2020.

[29] G. Testa, G. Zaccaria, M. Montanino et al., "Infrastructure-level traffic micro-simulation for probabilistic analysis of bridge loads," *Computer-Aided Civil and Infrastructure Engineering*, vol. 38, no. 9, pp. 1217–1235, 2023.

[30] J. Y. Zhou, C. C. Caprani, and L. W. Zhang, "On the structural safety of long-span bridges under traffic loadings caused by maintenance works," *Engineering Structures*, vol. 240, Article ID 112407, 2021.

[31] B. Sun, Y. L. Xu, F. Y. Wang, Z. X. Li, and Q. Zhu, "Multi-scale fatigue damage prognosis for long-span steel bridges under vehicle loading," *Structure and infrastructure engineering*, vol. 15, no. 4, pp. 524–538, 2019.

[32] J. Y. Zhou, Z. N. Zhou, L. W. Zhang, J. P. Zhang, and X. F. Shi, "Traffic-induced vibrations at the wet joint during the widening of concrete bridges and non-interruption traffic control strategies," *Computers and Concrete*, vol. 32, no. 4, pp. 411–423, 2023.

[33] X. Wang, R. Jiang, L. Li, Y. L. Lin, X. H. Zheng, and F. Y. Wang, "Capturing car-following behaviors by deep learning," *IEEE Transactions on Intelligent Transportation Systems*, vol. 19, no. 3, pp. 910–920, 2018.

[34] Us Department of Transportation – Fhwa, "NGSIM-next generation SIMulation," https://ops.fhwa.dot.gov/trafficanalysistools/ngsim.htm.

[35] Z. B. He, L. Zheng, and W. Guan, "A simple nonparametric car-following model driven by field data," *Transportation Research Part B: Methodological*, vol. 80, pp. 185–201, 2015.

[36] D. L. Wei and H. C. Liu, "Analysis of asymmetric driving behavior using a self-learning approach," *Transportation Research Part B: Methodological*, vol. 47, pp. 1–14, 2013.

[37] S. Panwai and H. Dia, "Neural agent car-following models," *IEEE Transactions on Intelligent Transportation Systems*, vol. 8, no. 1, pp. 60–70, 2007.

[38] M. F. Zhou, X. B. Qu, and X. P. Li, "A recurrent neural network based microscopic car following model to predict traffic oscillation," *Transportation Research Part C: Emerging Technologies*, vol. 84, pp. 245–264, 2017.

[39] X. L. Huang, J. Sun, and J. Sun, "A car-following model considering asymmetric driving behavior based on long short-term memory neural networks," *Transportation Research Part C: Emerging Technologies*, vol. 95, pp. 346–362, 2018.

[40] Y. X. Lin, P. Wang, Y. Zhou, F. Ding, C. Wang, and H. C. Tan, "Platoon trajectories generation: a unidirectional interconnected lstm-based car-following model," *IEEE Transactions on Intelligent Transportation Systems*, vol. 23, no. 3, pp. 2071–2081, 2022.

[41] X. Wang, R. Jiang, L. Li, Y. L. Lin, and F. Y. Wang, "Long memory is important: a test study on deep-learning based

car-following model," *Physica A: Statistical Mechanics and Its Applications*, vol. 514, pp. 786–795, 2019.

[42] L. J. Ma and S. R. Qu, "A sequence to sequence learning based car-following model for multi-step predictions considering reaction delay," *Transportation Research Part C: Emerging Technologies*, vol. 120, Article ID 102785, 2020.

[43] Y. Kang, G. Kim, S. Jeong, and K. Sohn, "Trajectory-based embedding for random coefficients of a theory-based car-following model," *Transportation Research Part C: Emerging Technologies*, vol. 152, Article ID 104183, 2023.

[44] Y. Pan, D. L. Wang, Y. Q. Dong, and B. Peng, "A novel vision-based framework for identifying dynamic vehicle loads on long-span bridges: a case study of jiangyin bridge, China," *IEEE Transactions on Intelligent Transportation Systems*, vol. 23, no. 8, pp. 10441–10457, 2022.

[45] Y. Q. Dong, D. L. Wang, Y. Pan, and Y. L. Ma, "Large field monitoring system of vehicle load on long-span bridge based on the fusion of multiple vision and wim data," *Automation in Construction*, vol. 154, Article ID 104985, 2023.

[46] Y. LeCun, Y. Bengio, and G. Hinton, "Deep learning," *Nature*, vol. 521, no. 7553, pp. 436–444, 2015.

[47] A. Vaswani, N. Shazeer, N. Parmar et al., "Attention is all you need," *Advances in Neural Information Processing Systems*, vol. 30, pp. 1–11, 2017.

[48] H. Y. Zhou, S. H. Zhang, J. Q. Peng et al., "Informer: beyond efficient transformer for long sequence time-series forecasting," in *Proceedings of the Thirty-Fifth AAAI Conference on Artificial Intelligence*, pp. 11106–11115, Vancouver, Canada, February 2021.

[49] M. H. Chen, H. W. Peng, J. L. Fu, and H. B. Ling, "Autoformer: searching transformers for visual recognition," in *Proceedings of the 2021 IEEE/CVF International Conference on Computer Vision (ICCV 2021)*, pp. 12250–12260, Montreal, QC, Canada, October 2021.

[50] V. Punzo, M. T. Borzacchiello, and B. Ciuffo, "On the assessment of vehicle trajectory data accuracy and application to the next generation simulation (ngsim) program data," *Transportation Research Part C: Emerging Technologies*, vol. 19, no. 6, pp. 1243–1262, 2011.

[51] M. Montanino and V. Punzo, "Trajectory data reconstruction and simulation-based validation against macroscopic traffic patterns," *Transportation Research Part B: Methodological*, vol. 80, pp. 82–106, 2015.

[52] D. Z. Han, T. Guo, L. Y. Huang, and Z. X. Liu, "A study on longitudinal displacements and damage control of expansion joints of long-span steel bridges under stochastic traffic loads," *Journal of Vibration and Shock*, vol. 38, no. 24, pp. 172–178, 2019.

[53] J. X. Mao, H. Wang, and J. Li, "Bayesian finite element model updating of a long-span suspension bridge utilizing hybrid Monte Carlo simulation and kriging predictor," *KSCE Journal of Civil Engineering*, vol. 24, no. 2, pp. 569–579, 2020.

[54] A. J. Smola and B. Schölkopf, "A tutorial on support vector regression," *Statistics and Computing*, vol. 14, no. 3, pp. 199–222, 2004.

[55] G. Q. Zhang, B. Eddy Patuwo, and M. Y Hu, "Forecasting with artificial neural networks," *International Journal of Forecasting*, vol. 14, no. 1, pp. 35–62, 1998.

[56] S. Hochreiter and J. Schmidhuber, "Long short-term memory," *Neural Computation*, vol. 9, no. 8, pp. 1735–1780, 1997.

[57] K. Cho, B. V. Merrienboer, Ç. Gülçehre, F. Bougares, H. Schwenk, and Y. Bengio, "Learning phrase representations using RNN encoder-decoder for statistical machine translation," 2014, https://arxiv.org/abs/1406.1078.

[58] I. Sutskever, O. Vinyals, and Q. V. Le, "Sequence to sequence learning with neural networks," 2014, https://arxiv.org/abs/1409.3215.

[59] Z. Zhang, R. J. Ma, and B. Hua, "Vehicle loading and effects on orthotropic steel deck of runyang bridge based on wim data," in *Proceedings of the 8th International Conference on Bridge Maintenance, Safety and Management (IABMAS)*, pp. 393–399, Paraná, Brazil, June 2016.